X-ray diffraction study of the phase transition of $K_2Mn_2(BeF_4)_3$: a new type of low-temperature structure for langbeinites

A. Guelylah,[a]* G. Madariaga,[a] V. Petricek,[b] T. Breczewski,[c] M. I. Aroyo[a]† and E. H. Bocanegra[c]

[a]Departamento de Física de la Materia Condensada, Facultad de Ciencias, Universidad del País Vasco, Apartado 644, Bilbao 48080, Spain, [b]Institute of Physics, Czech Academy of Sciences, Cukrovarnicka 10, 162 00 Praha 6, Czech Republic, and [c]Departamento de Física Aplicada II, Facultad de Ciencias, Universidad del País Vasco, Apartado 644, Bilbao 48080, Spain

† On leave of absence from the Faculty of Physics, University of Sofia, Sofia, Bulgaria.

Correspondence e-mail: wmbgugua@lg.ehu.es

The potassium manganese tetrafluoroberyllate langbeinite compound has been studied in the temperature range 100–300 K. Using DSC measurements, a phase transition has been detected at 213 K. The space group of the low-temperature phase was determined to be $P112_1$ using X-ray diffraction experiments and optical observations of the domain structure. The **b** axis is doubled with respect to the prototypic $P2_13$ cubic phase. Lattice parameters were determined by powder diffraction data [$a = 10.0690 (8)$, $b = 20.136 (2)$, $c = 10.0329 (4)$ Å, $\gamma = 90.01 (1)°$]. A precise analysis of the BeF_4 tetrahedra in the low-temperature phase shows that two independent tetrahedra rotate in opposite directions along the doubled crystallographic axis. A symmetry mode analysis of the monoclinic distortion is also reported. This is the first report of the existence of such a phase transition in $K_2Mn_2(BeF_4)_3$ and also of a new type of low-temperature structure for langbeinite compounds.

1. Introduction

Sulfates with crystal structures of the langbeinite type $A_2B_2(SO_4)_3$ have attracted much interest in recent years given the ferroelastic [$K_2Cd_2(SO_4)_3$ (KCdS) and $K_2Mn_2(SO_4)_3$ (KMnS); Abrahams & Bernstein, 1977; Maeda, 1979] and ferroelectric {$(NH_4)_2Cd_2(SO_4)_3$ [$(NH_4)CdS$] and $Tl_2Cd_2(SO_4)_3$ (TCdS); Jona & Pepinsky, 1956; Brezina & Glogarova, 1972; Glogarova *et al.*, 1972} character of their structural phase transitions. Langbeinite compounds were classified into two types according to their phase transition scheme. Crystals that exhibit a series of phase transitions from the cubic ($P2_13$) high-temperature phase to an orthorhombic ($P2_12_12_1$) phase across two intermediate phases, monoclinic ($P2_1$) and triclinic ($P1$), belong to type I. Crystals of type II undergo a single phase transition from the cubic ($P2_13$) to the orthorhombic ($P2_12_12_1$) phase. In both cases all low-temperature phases are ferroelastic, with the monoclinic and the triclinic phases also being ferroelectric. Recent works on langbeinites have concentrated on the understanding of the $P2_13$–$P2_12_12_1$ phase-transition mechanism. However, structural investigations of the low-temperature phases on type I langbeinite have not been carried out owing to the experimental difficulties arising from the presence of a high number of twin domains. Only recently have the structure of the monoclinic and orthorhombic phases in TCdS been solved (Guelylah *et al.*, 2000). This work revealed some mechanisms, responsible for the phase transitions sequence, which are different from those observed in type II langbeinite.

Besides sulfate langbeinites, other langbeinite compounds exist with the same combination of monovalent and divalent

cations but different tetrahedral groups, for instance: $(BeF_4)^{2-}$, $(SeO_4)^{2-}$, $(CrO_4)^{2-}$ or $(PO_4)^{2-}$ (Aleonard & Le Fur, 1967; Genty et al., 1968; Le Fur & Aleonard, 1969; Kohler & Franke, 1964; Cord et al., 1971; Leclaire et al., 1989).

On some langbeinite compounds with sulfate groups, it was proved experimentally that a change in the monovalent cation provokes change in the phase transition scheme (for example, TCdS and KCdS differ in the monovalent cation only, but their phase transition schemes are different; Brezina & Glogarova, 1972; Abrahams & Bernstein, 1977; Abrahams et al., 1978). However, compounds with tetrahedral groups other than SO_4 have never been the objective of experimental studies searching structural phase transitions.

Owing to the similar size of BeF_4 and SO_4 tetrahedra, BeF_4-based langbeinites were selected for our study, looking for new structural features in this family. The only works reported on tetrafluoroberyllate langbeinite compounds were carried out by the end of the sixties (Aleonard & Le Fur, 1967; Genty et al., 1968; Le Fur & Aleonard, 1969). These studies (see Table 1) determined the symmetry, lattice constant and (some of them) the structure at room temperature (by powder X-ray diffraction) of several BeF_4 langbeinites.

The langbeinite $K_2Mn_2(BeF_4)_3$ (KMnB) presents a phase transition at approximately 213 K. Below this temperature, KMnB shows a crystal structure (with double unit-cell volume) different from that of any other low-temperature phase reported in the literature for a langbeinite. The structure at room temperature was determined previously (Guelylah, Breczewski & Madariaga, 1996) by single-crystal X-ray diffraction. The aim of the present work is the determination of the low-temperature phase structure and a comparison with the low-temperature phases of other sulfate langbeinites.

2. Experimental

Single crystals of KMnB were grown from saturated aqueous solution at 357 K. The technique used has been described
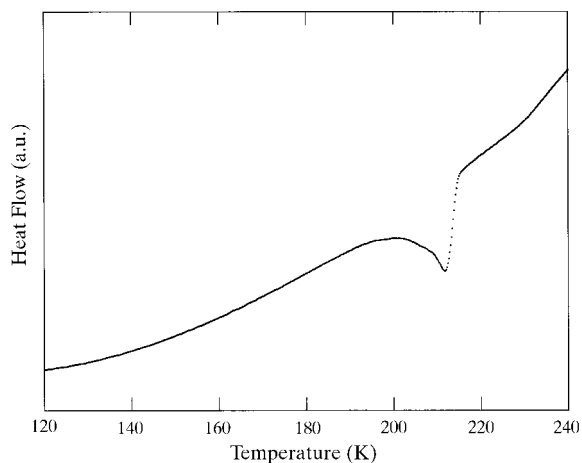

Figure 1
DSC curve of $K_2Mn_2(BeF_4)_3$, showing the phase transition observed at 213 K.

Table 1
Schematic representation of the $A_2^+B_2^{2+}(BeF_4)_3$ compounds.

The lattice parameter (space group $P2_13$) determined at room temperature as well as the corresponding reference are shown for known compounds. Asterisks indicate the compounds whose structure was determined by X-ray powder diffraction. The ionic radii (R) are listed for each cation. /1/, /2/ and /3/ refer to the works of Le Fur & Aleonard (1969), Genty et al. (1968) and Aleonard & Le Fur (1967), respectively.

B^{2+} A^+, R (Å)	Mg^{2+} 0.66	Ni^{2+} 0.69	Co^{2+} 0.74	Zn^{2+} 0.74	Mn^{2+} 0.80	Cd^{2+} 0.97	Ca^{2+} 0.99
Cs^+ 1.67						10.55 Å /2/	10.67 Å * /1,2/
Tl^+ 1.48			10.07 Å /2/		10.25 Å /2/	10.40 Å /2/	
Rb^+ 1.47						10.38 Å * /1/	
NH_4^+ 1.43	9.96 Å /2/		10.05 Å /2/	10.04 Å * /1,2/	10.21 Å /2/		
K^+ 1.33	9.8 Å * /1,3/	9.88 Å /3/	9.96 Å /3/	9.93 Å * /1,3/	10.10 Å /3/		

previously (Guelylah, Breczewski & Madariaga, 1996). Differential scanning calorimetry measurements carried out in the temperature range 100–300 K show (Fig. 1) a phase transition at 213 K. The observed thermal hysteresis (~3°) indicates the first-order character of the phase transition. This phase transition temperature appears slightly higher than that of KMnS (Yamada, Maedo & Adachi, 1981), which belongs to type II langbenites and differs only in the tetrahedral group.

The sample used for X-ray precession photographs was ground into a sphere of radius 0.2 mm. Precession photographs (exposure time 20 h with filtered Cu $K\alpha$ radiation) were taken at 293 K (zeroth and first layers) and 180 K (up to the second layer). For the data collection at 177 K a sphere of radius 0.14 (1) mm was mounted in an Enraf–Nonius CAD-4 diffractometer. The temperature was controlled with an Oxford Cryosystem open gas-flow cryostat (Cosier & Glazer, 1986). Temperature stability was within ±0.2 K during the time of the measurements. Owing to the domain structure of the low-temperature phase and the doubling of its unit cell volume, the unit cell used for the data collection was pseudo-cubic with the three crystallographic axes doubled with respect to those of the high-temperature cubic unit cell ($a' \simeq b' \simeq c' \simeq 20.1$ Å, $\alpha \simeq \beta \simeq \gamma \simeq 90°$). Data collection and refinement parameters are listed in Table 2.

Below the phase transition, some reflections, belonging to the different twin domains, share approximately reciprocal points. Given the monoclinic distortion, the superposition of intensities is not necessarily exact and therefore the lattice parameters determined from a twinned sample are biased by this systematic error, since the diffractometer will centre the (multiple) Bragg peaks at the centroid of the superimposed reflections. For these reasons we report here the unit-cell parameters of the low-temperature phase at 177 K obtained by powder diffraction measurements. Powder measurements were performed on a Stoe focusing monochromatic beam

Table 2
Data collection and refinement parameters for $K_2Mn_2(BeF_4)_3$ at 177 K.

Crystal data	
Chemical formula	$K_2Mn_2(BeF_4)_3$
Chemical formula weight	443.11
Cell setting	Monoclinic
Space group	$P112_1$
a (Å)	10.0690 (8)
b (Å)	20.136 (2)
c (Å)	10.0329 (4)
γ (°)	90.01 (1)
V (Å^3)	2030.34 (2)
Z	8
D_x (Mg m^{-3})	2.893
Radiation type	Mo $K\alpha$
Wavelength (Å)	0.71073
No. of reflections for orientation matrix	25
θ range (°)	7–13
Determination of cell parameters	Powder diffraction
θ range (°)	4.41–29.97
μ (mm^{-1})	3.449
Temperature (K)	177
Crystal form	Spherical
Crystal radius (mm)	0.14 (1)
Crystal color	Light pink
Data collection	
Diffractometer	Enraf–Nonius CAD-4
Monochromator	Graphite
Data collection method	$\theta/2\theta$ scans
Absorption correction	Sphere
T_{max}/T_{min}	0.512/0.502
No. of measured reflections	19 227
No. of independent reflection	12 644
No. of observed reflections [$I > 3\sigma(I)$]	8783
R_{int}	0.027
$\sin(\theta/\lambda)_{max}$ (Å^{-1})	0.7001
θ max (°)	29.84
Range of h, k, l	$-14 \rightarrow h \rightarrow 14$
	$-28 \rightarrow k \rightarrow 28,$
	$-14 \rightarrow l \rightarrow 14$
No. of standard reflections	3
Frequency of standard reflections	Every 60 min
Intensity decay (%)	5
Refinement	
Refinement on	F
R	0.064
wR	0.055
S	3.26
R_{all}	0.119
wR_{all}	0.056
S_{all}	3.75
No. of reflection used on refinement	12 644
No. of parameters used	260
Weighting scheme	$w = 1/\sigma^2(F)$
$(\Delta/\sigma)_{max}$	0.0003
$\Delta\rho^1_{max}$ (e Å^{-3})	12.2
$\Delta\rho^1_{min}$ (e Å^{-3})	-12.2
$\Delta\rho^2_{max}$ (e Å^{-3})	5.14
$\Delta\rho^2_{min}$ (e Å^{-3})	-5.40
Domain fractions	
f_1	0.1549 (8)
f_2	0.2094 (8)
f_3	0.2144 (9)
f_4	0.1369 (7)
f_5	0.1738 (7)
f_6	0.1105 (7)

Computer programs used: *CAD*-4*VPC* (Enraf–Nonius, 1989), *Fullprof* (Rodriguez-Carvajal, 1990), *JANA*98 (Petricek & Dusek, 1998).

Table 3
Twin relationship expressed in the doubled pseudo-monoclinic unit cell $a' = a$, $b' = 2b$, $c' = c$.

$$\begin{bmatrix} h \\ k \\ l \end{bmatrix}^1 = \begin{bmatrix} 1 & 0 & 0 \\ 0 & 1 & 0 \\ 0 & 0 & 1 \end{bmatrix} \begin{bmatrix} h \\ k \\ l \end{bmatrix}^1 \qquad \begin{bmatrix} h \\ k \\ l \end{bmatrix}^4 = \begin{bmatrix} -1 & 0 & 0 \\ 0 & 1 & 0 \\ 0 & 0 & -1 \end{bmatrix} \begin{bmatrix} h \\ k \\ l \end{bmatrix}^1$$

$$\begin{bmatrix} h \\ k \\ l \end{bmatrix}^2 = \begin{bmatrix} 0 & 0 & 1 \\ \frac{1}{2} & 0 & 0 \\ 0 & 2 & 0 \end{bmatrix} \begin{bmatrix} h \\ k \\ l \end{bmatrix}^1 \qquad \begin{bmatrix} h \\ k \\ l \end{bmatrix}^5 = \begin{bmatrix} 0 & 0 & -1 \\ \frac{1}{2} & 0 & 0 \\ 0 & -2 & 0 \end{bmatrix} \begin{bmatrix} h \\ k \\ l \end{bmatrix}^1$$

$$\begin{bmatrix} h \\ k \\ l \end{bmatrix}^3 = \begin{bmatrix} 0 & 2 & 0 \\ 0 & 0 & \frac{1}{2} \\ 1 & 0 & 0 \end{bmatrix} \begin{bmatrix} h \\ k \\ l \end{bmatrix}^1 \qquad \begin{bmatrix} h \\ k \\ l \end{bmatrix}^6 = \begin{bmatrix} 0 & 2 & 0 \\ 0 & 0 & -\frac{1}{2} \\ -1 & 0 & 0 \end{bmatrix} \begin{bmatrix} h \\ k \\ l \end{bmatrix}^1$$

transmission diffractometer equipped with a linear position detector. The powdered samples were inserted in a Lindemann capillary of diameter 0.3 mm. The measured region was 5.00–69.94° (2θ). λ(Cu $K\alpha_1$) = 1.54056 Å. Lattice parameters were refined using the program *Fullprof* (Rodriguez-Carvajal, 1990). Atomic positional parameters for profile refinement were extrapolated from the known room-temperature cubic structure. This refinement was also useful to check the goodness of the structural model for further single-crystal refinements. Final lattice parameters after least-squares refinement are $a = 10.0690$ (8), $b = 20.136$ (2), $c = 10.0329$ (4) Å and $\gamma = 90.01$ (1)°. Final agreement factors are $R_p = 0.0161$, $R_{wp} = 0.0218$, $R_{exp} = 0.0238$, $R_{Bragg} = 0.0911$ and $R_F = 0.0830$.

3. Results and discussion

3.1. Space-group determination

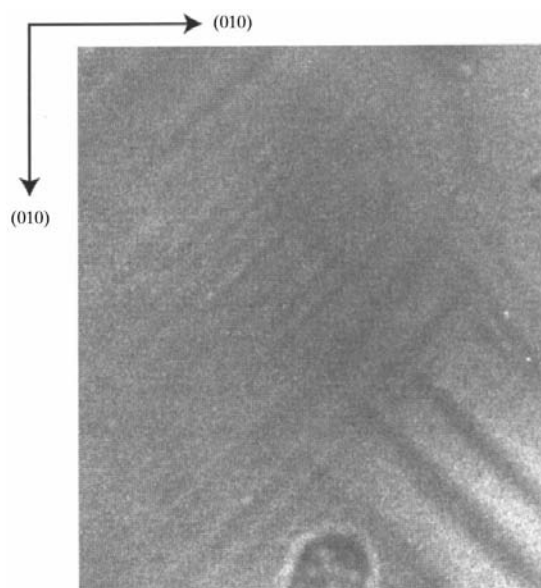The space group of the low-temperature phase was determined by X-ray precession photographs in combination with

Figure 2
Domain structure observed in the low-temperature phase of $K_2Mn_2(BeF_4)_3$ at 180 K.
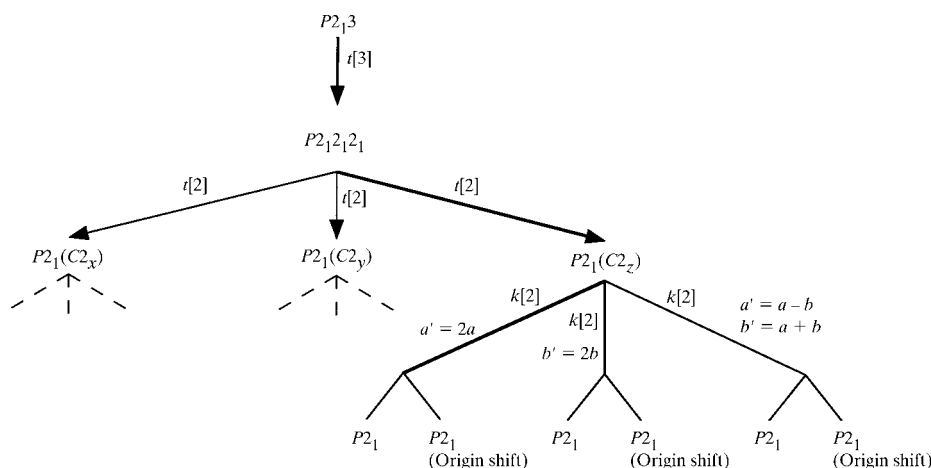
Figure 3
Lattice of maximal subgroups for $P2_13 > P2_1(2\mathbf{b})$. The symbols $k[2]$ and $t[2]$ indicate the type (k for klassengleiche and t for translationengleiche) and the index of the corresponding maximal subgroups. The heavy lines connect the two possible monoclinic structures for which the unit-cell volume is doubled.
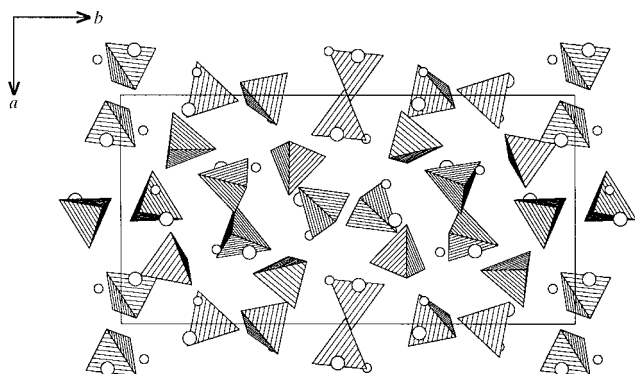

Figure 4
Projection along (001) of the monoclinic structure of $K_2Mn_2(BeF_4)_3$ at 177 K, showing the SO_4 tetrahedra, K atoms (large circles) and Mn atoms (small circles).

the optical observation of domain structure. Owing to the lack of large single crystals, the multidomain structure was analysed in small samples of ~ 1.5 mm$^2 \times 0.3$ mm.

3.1.1. X-ray precession photographs. X-ray precession photographs of KMnB at room temperature showed no difference with respect to the high-temperature cubic phase of sulfate langbeinites. However, at 180 K, the zeroth layer[1] shows important changes. The presence of new reflections indicates a new phase with a unit cell doubled along all the crystallographic axes. Owing to the domain structure direct assignation of the space group from the detected systematic absences was impossible. The precession photographs of the first layers ($1kl$ and $h1l$) corresponding to a multiple cell ($a' = 2a$ and $b' = 2b$) do not show superlattice reflections related to the duplication and are very similar to those obtained at room temperature. Therefore, the duplication only

occurs along one of the crystallographic axes and the appearance of superlattice reflections along the three directions in the zeroth layers is due to the superposition of three reciprocal lattices related by the threefold axes lost in the phase transition. All the layers with h and/or k equal to $2n$ (n integer) with respect to the reciprocal basis corresponding to the doubled cell show the same aspect.

The possible space groups compatible with these results are $P1$, $P2$, $P2_1$ (with interaxial angles approximately equal to 90°), $P222$, $P2_122$ and $P2_12_12$. All of them must be accompanied with a duplication along one of the crystal axes (a, b or c), which must not be parallel to a twofold screw axis (if any).

3.1.2. Optical observation of the domain structure. The cubic phase observed down to 213 K is optically isotropic. Below the phase transition temperature it splits into several domains. Fig. 2 shows a photomicrograph of the domain pattern observed at 180 K. Looking along a pseudo-cubic [001] direction (Fig. 2), we can see a domain pattern which consists of stripes situated at approximately 45° (or $-45°$) with respect to the pseudo-cubic axis [100]. The boundaries between these stripes are the planes (110) [or ($1\bar{1}0$)]. This domain configuration, also observed in the monoclinic phases of $(NH_4)CdS$ (Glogarova et al., 1972) and TCdS (Brezina & Glogarova, 1972) suggests that the low-temperature phase of KMnB is probably monoclinic and, therefore, ferroelectric.

Assuming that the phase transition in KMnB is, as for type I langbeinites, $P2_13 \leftrightarrow P2_1$, the number of orientation states for the low-temperature phase will be 6. The six domains, $\pm x_i$ ($i = 1, 2, 3$),[2] are related by the symmetry elements lost in the phase transition. One of the stripes in Fig. 2 corresponds to a couple of the antiparallel domains $+x_3$ and $-x_3$ related by a twofold axis (C_{2x} or C_{2y}) perpendicular to the polar axis and separated by (010) and (100) domain walls (Sapriel, 1975), while the neighboring ones are $\pm x_1$ or $\pm x_2$ domains. The domain boundaries separating the $\pm x_3$ and $\pm x_1$ (or $\pm x_2$) domains are (110) or ($1\bar{1}0$). Therefore, the structure of the domain patterns observed leads us to conclude that the symmetry of the low-temperature phase of KMnB is monoclinic.

Furthermore, Dvorák (1974), based on group theoretical calculations, predicted that an instability corresponding to the point $X(\frac{1}{2}\ 0\ 0)$ of the first Brillouin zone may induce a homogeneous $P2_1$ phase with a unit cell doubled along the $\mathbf{a}$ axis or doubled along both the $\mathbf{a}$ and $\mathbf{b}$ axes. The precession photographs coincide with the former prediction of Dvorák,

---

[1] Supplementary data for this paper are available from the IUCr electronic archives (Reference: CK0001). Services for accessing these data are described at the back of the journal.

[2] $\pm x_i$ represents the domain whose polar axis is along the cubic axis $\pm\mathbf{a}$, $\pm\mathbf{b}$ and $\pm\mathbf{c}$ for $i = 1, 2$ and 3, respectively.

Table 4
Bond-valence sums of K, Mn and Be atoms in the monoclinic (177 K) and cubic structures of $K_2Mn_2(BeF_4)_3$ with s.u. in parentheses.

Monoclinic phase (177 K)		Cubic phase (Guelylah, Breczewski & Madariaga, 1996)	
K11	0.86 (2)	K1	0.68 (2)
K12	0.87 (2)		
K13	0.77 (2)		
K14	0.77 (2)		
K21	0.65 (2)	K2	0.65 (2)
K22	0.65 (2)		
K23	0.80 (2)		
K24	0.89 (2)		
Mn11	2.04 (4)	Mn1	2.08 (4)
Mn12	2.05 (4)		
Mn13	2.02 (4)		
Mn14	1.89 (4)		
Mn21	2.02 (4)	Mn2	2.04 (4)
Mn22	1.84 (4)		
Mn23	1.96 (4)		
Mn24	2.05 (4)		
Be	2.02 (5)	Be	2.12 (5)

so the space group $P2_1$ can be assigned to the low-temperature phase of KMnB.

3.2. Structure description

According to the above results and given the maximal subgroup chain of the $P2_13$ space group (Fig. 3), there are two possible directions (**a** or **b**) for the doubling. The corresponding structural models were refined in order to check which of them is correct for the low-temperature phase. In both cases the starting models were extrapolated from the structure determined at room temperature (293 K; Guelylah, Breczewski & Madariaga, 1996). These models were
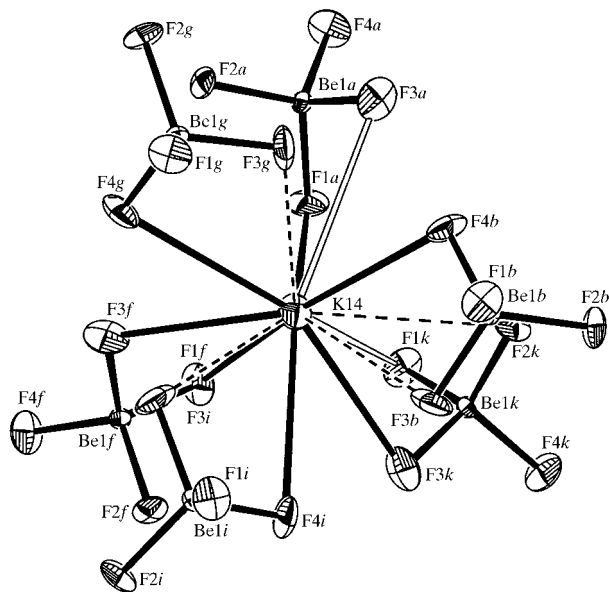

Figure 5
Contact reconstruction around the K14 atom in $K_2Mn_2(BeF_4)_3$ at 177 K. The dashed lines represent the new established contacts with respect to the cubic phase, while the open bonds are those lost in the phase transition.

previously checked using the Rietveld method as explained above. The twin operations which relate the Miller indices corresponding to the superimposed intensities of the different orientation states present in this phase are listed in Table 3 for the '2b' model. The initial values of the domain fractions were the same for all the orientation states (1/6).

In the beginning of the refinement the atoms forming the $(BeF_4)^{2-}$ groups were refined freely. Nevertheless, this gives rise to a deformed structure with some interatomic distances out of their chemically reasonable limits. Taking into account the quasi-rigid behavior of the tetrahedral group in langbeinite compounds (Abrahams et al., 1978; Yamada, Maeda & Adachi, 1981), the geometry of the $(BeF_4)^{2-}$ anion was taken to be identical for all the tetrahedral groups through the so-called model molecules. $(BeF_4)^{2-}$ is not considered strictly rigid, because its geometry can change during the refinement (Petricek & Dusek, 1998). The position of each $(BeF_4)^{2-}$ group is determined by three rotations and three translations which are refined together with the atomic temperature parameters.

During the refinement of the '2a' model the anisotropic temperature factors of some K and Mn atoms became non-positive definite. Therefore, the atoms which occupied the same position in two successive cubic unit cells along the **a** direction were refined with identical temperature factors. Even with this type of restriction the temperature factors of some Mn continue being non-positive definite. Thus, Mn atoms were refined isotropically. The isotropic refinement of the Mn atoms and the restrictions on the temperature factors for K atoms together with the molecular restriction in the (BeF_4) geometry increased the R value, although the atomic positions were slightly affected. Final R/wR values were 0.090/0.097 for this model.

In the case of the '2b' model, all atoms could be refined anisotropically. The anisotropic temperature parameters for those atoms occupying the same position (x, z) along the b axis in the cubic phase were refined without any restriction and the final solution showed significantly better results than the previous '2a' model. Final R/wR values are 0.064/0.055. Final domain fractions are listed in Table 2. The sum of the volume fractions for each couple of antiparallel domains represents approximately the third part of the total volume of the crystal. Fig. 4 shows the structure of KMnB at 177 K projected along the (001) direction.

The final difference-Fourier synthesis[3] inevitably results (as usual for twinned samples) in rather high electron-density values that are given in Table 2 as $\Delta\rho^1$. Another possibility for calculating the residual electron densities is based on the relation $|F_o|_1 = (Y_o/Y_c)^{1/2}|F_c|_1$, where Y_o and Y_c are the scaled observed and calculated intensities, and $|F_o|_1$ and $|F_c|_1$ are the 'observed' and calculated moduli of the structure factors for the first domain. Unlike the first modification for

---

[3] $\Delta\rho^1 = V^{-1}\Sigma_h \Delta F_1(\mathbf{h}) \exp(-2\pi i\mathbf{hr})$, where $\Delta F_1(\mathbf{h})$ is defined for a multiply twinned crystal composed from N domains as $\Delta F_1(\mathbf{h}) = \{[(|F_o|^2/S_c^2) - \sum_{i=2}^{N} f_i |F_c|_i^2]/f_1\} - |F_c|_1$, where f_i and $|F_c|_i$ are the volume fraction and the modulus of the calculated structure factors of the ith domain, respectively.

Table 5
Translations in relative units and rotations (°) of the BeF_4 tetrahedra in the monoclinic structure at 177 K with respect to the room-temperature structure.

The pairs of tetrahedra $[(BeF_4)a, (BeF_4)b]$, $[(BeF_4)c, (BeF_4)d]$, $[(BeF_4)e, (BeF_4)f]$, $[(BeF_4)g, (BeF_4)h]$, $[(BeF_4)i, (BeF_4)j]$ and $[(BeF_4)k, (BeF_4)l]$ are related between them by a translation of $(0 \frac{1}{2} 0)$.

	Rx	Ry	Rz	Tx	Ty	Tz
$(BeF_4)a$	−9.865	3.502	3.519	1.858×10^{-2}	8.768×10^{-3}	-1.181×10^{-3}
$(BeF_4)b$	4.222	−9.166	−4.060	1.716×10^{-2}	5.398×10^{-3}	-1.706×10^{-2}
$(BeF_4)c$	−0.258	−13.303	3.199	-7.830×10^{-3}	5.739×10^{-3}	-6.194×10^{-3}
$(BeF_4)d$	15.507	10.312	10.613	7.228×10^{-3}	-5.550×10^{-4}	-2.654×10^{-3}
$(BeF_4)e$	−8.396	−11.160	8.879	-7.157×10^{-3}	-4.800×10^{-4}	-1.241×10^{-2}
$(BeF_4)f$	11.881	0.617	11.299	-2.612×10^{-3}	-8.582×10^{-3}	-1.677×10^{-2}
$(BeF_4)g$	0.308	6.168	10.573	-4.398×10^{-3}	2.674×10^{-3}	3.804×10^{-3}
$(BeF_4)h$	5.544	−17.762	−7.363	1.002×10^{-2}	-1.162×10^{-2}	1.332×10^{-2}
$(BeF_4)i$	−13.369	0.008	8.441	-3.271×10^{-3}	1.895×10^{-3}	-3.900×10^{-3}
$(BeF_4)j$	9.674	10.557	16.689	-5.663×10^{-3}	6.425×10^{-3}	-6.898×10^{-3}
$(BeF_4)k$	−11.028	7.555	−11.327	9.095×10^{-3}	3.423×10^{-4}	1.623×10^{-3}
$(BeF_4)l$	8.459	−8.085	7.129	-1.053×10^{-2}	5.879×10^{-3}	-1.162×10^{-2}

$\Delta\rho$, the second one assumes that the disagreement between $(Y_o)^{1/2}$ and $(Y_c)^{1/2}$ is equally distributed among all domains. The corresponding residuals are given in Table 2 as $\Delta\rho^2$. Irrespective of their absolute value the highest maxima and the deepest minima were located near the Mn atoms.

Like the cubic phase, the monoclinic structure is constituted of (BeF_4) tetrahedra and distorted polyhedra around the metal atoms (K and Mn). BeF_4 groups present on average a regular form with Be—F distances varying from 1.527 (6) to 1.545 (7) Å and a mean value of 1.534 (7) Å; the F—Be—F angles vary from 105.5 (4) to 111.2 (4)° with a mean value of 109.4 (4)°. Nearest neighbor F atoms form distorted octahedra

Figure 6
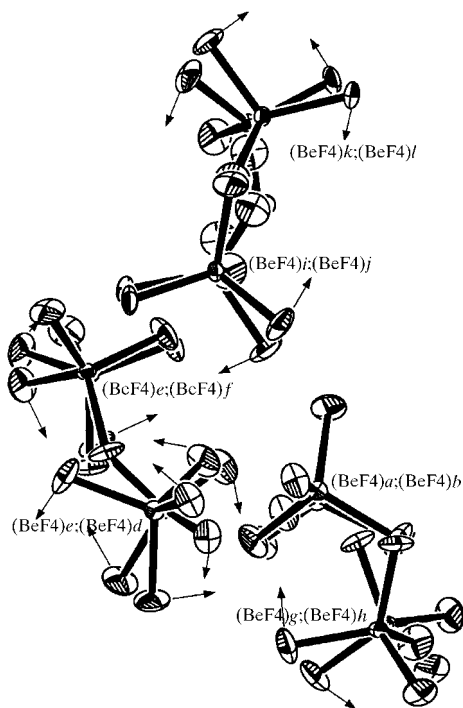Projection along (010) of the asymmetric unit of $K_2Mn_2(BeF_4)_3$ at 177 K, showing the rotation of the BeF_4 tetrahedra. The most important displacements are indicated by arrows.

around Mn^{2+} atoms, with an average Mn—F distance that appears to increase slightly with respect to that of the cubic phase. The Mn cations as in the cubic phase are not at the center of their coordination octahedra, but they are shifted toward the F2 (for Mn2i, i = 1, 2, 3, 4) and F4 (for Mn1i, i = 1, 2, 3, 4) triangles. This off-centring parameter is, in general, slightly larger in the monoclinic phase than in the cubic one. Nevertheless, the shift of some Mn cations is up to two times the shift they show in the cubic phase. Fluorine–manganese contacts are neither broken nor created at the phase transition.

The coordination about K atoms is 9 in the cubic phase. In the monoclinic phase it ranges from 7 to 11 within a sphere of 3.25 Å. The rotation of the (BeF_4) groups together with the displacement of K ions are sufficient to make new and break previous K—F contacts. The coordination about K14 and K23 is 11. K14 loses two cubic contacts and makes four new contacts (Fig. 5), while K23 establishes three new contacts and breaks one. K11 is surrounded by ten F atoms, breaks two cubic contacts and makes three new ones in the monoclinic phase. The coordination around K21 and K22 is lower than in the cubic phase; they lose three and two cubic K—F contacts, respectively, and establish only one new contact. The coordination of the remaining K cations is 9. K12 makes two new contacts and breaks another two, and K13 breaks one cubic contact and establishes a new one. K24 continues with the same contacts as in the cubic phase.

The bond-valence sums (Brown & Altermatt, 1985; Brese & O'Keeffe, 1991; Table 4) show a notable improvement for $(K1i)^+$ cations (i = 1, 2, 3 and 4) with respect to the cubic phase. However, for K2i cations, such improvement is observed only for K23 and K24, while K21 and K22 are still loosely bonded. The bond-valence sums in the monoclinic structure for the rest of the cations and anions (Mn^{2+}, Be^{2+} and F^-) are approximately equal to the valence of these ions.

3.3. Rotation of BeF_4 tetrahedra

A quantitative analysis of the atomic coordinates in the monoclinic structure of KMnB indicates a displacement of all atoms with respect to the room-temperature structure. A more consistent analysis of the displacement of the BeF_4 groups in the monoclinic phase can be performed considering them explicitly as rigid units and therefore describing their displacements by rotations and translations of the whole group. The set of rigid translations and rotations along the crystallographic axes for each independent tetrahedral group were obtained from a least-squares fit and are listed in Table 5. BeF_4 rotations are quite important and of the same order of magnitude as those observed in type II sulfate langbeinites (KMnS, KCaS and KCdS) (Yamada, Maeda & Adachi, 1981;

Table 6
Chain-adapted symmetry modes compatible with the $P2_1$ ($b' = 2b$) symmetry for atoms in the 4(a) Wyckoff position of the $P2_13$ space group.

The first four atoms and the second four atoms are listed following the labeling scheme of the *International Tables for Crystallography* (1992, Vol. A). Each group of four atoms belong to a cubic unit cell.

	Atomic positions	$P2_13$ φ_1	$P2_12_12_1$ φ_2	φ_3	$P2_1$ (c axis) φ_4	φ_5	φ_6	$P2_1$ ($2b$) φ_7	φ_8	φ_9	φ_{10}	φ_{11}	φ_{12}
Zero cell	(1) x, x, x	111	$1\frac{1\bar{1}}{22}$	$01\bar{1}$	100	010	001	100	010	001	000	000	000
	(2) $\frac{1}{2}-x, -x, \frac{1}{2}+x$	$\bar{1}\bar{1}1$	$\bar{1}\frac{1}{2}\frac{\bar{1}}{2}$	$0\bar{1}\bar{1}$	$\bar{1}00$	$0\bar{1}0$	001	$\bar{1}00$	$0\bar{1}0$	001	000	000	000
	(3) $-x, \frac{1}{2}+x, \frac{1}{2}-x$	$\bar{1}1\bar{1}$	$1\frac{\bar{1}1}{22}$	011	100	$0\bar{1}0$	001	000	000	000	100	010	001
	(4) $\frac{1}{2}+x, \frac{1}{2}-x, -x$	$1\bar{1}\bar{1}$	$1\frac{11}{22}$	$0\bar{1}1$	$\bar{1}00$	010	001	000	000	000	$\bar{1}00$	$0\bar{1}0$	001
$+t(0, 1, 0)$	(5) $x, x+1, x$	111	$1\frac{1\bar{1}}{22}$	$01\bar{1}$	100	010	001	$\bar{1}00$	$0\bar{1}0$	$00\bar{1}$	000	000	000
	(6) $\frac{1}{2}-x, -x+1, \frac{1}{2}+x$	$\bar{1}\bar{1}1$	$1\frac{1\bar{1}}{22}$	$0\bar{1}\bar{1}$	$\bar{1}00$	$0\bar{1}0$	001	100	010	$00\bar{1}$	000	000	000
	(7) $-x, \frac{1}{2}+x+1, \frac{1}{2}-x$	$\bar{1}1\bar{1}$	$1\frac{\bar{1}1}{22}$	011	100	$0\bar{1}0$	001	000	000	000	$\bar{1}00$	$0\bar{1}0$	$00\bar{1}$
	(8) $\frac{1}{2}+x, \frac{1}{2}-x+1, -x$	$1\bar{1}\bar{1}$	$1\frac{11}{22}$	$0\bar{1}1$	$\bar{1}00$	010	001	000	000	000	100	010	$00\bar{1}$
	N	$(1/24)^{1/2}$	$(1/12)^{1/2}$	$(1/16)^{1/2}$	$(1/8)^{1/2}$	$(1/8)^{1/2}$	$(1/8)^{1/2}$	$\frac{1}{2}$	$\frac{1}{2}$	$\frac{1}{2}$	$\frac{1}{2}$	$\frac{1}{2}$	$\frac{1}{2}$

Speer & Salje, 1986; Lissalde *et al.*, 1979; Guelylah, Aroyo & Pérez-Mato, 1981). An analysis of the BeF$_4$ rotations shows that two tetrahedra occupying the same position in two adjacent cubic cells along the doubled **b** axis rotate in opposite directions around it (Fig. 6). These rotations together with K and Mn displacements seem to be the principal cause for the duplication of the **b** axis and the observed deformation of the K and Mn coordination polyhedra.

3.4. Distortion modes analysis

Our next step was to perform a *chain-adapted* symmetry mode analysis to separate the global structural distortion

relating the monoclinic and the cubic structures in primary (which trigger the transition) and secondary modes (Aroyo & Pérez-Mato, 1998). Examples of this type of analysis can be found in Aroyo & Pérez-Mato (1998), Rae *et al.* (1990) and Guelylah *et al.* (2000). In such an analysis the atomic displacement is decomposed in displacements whose symmetries appear in the group–subgroup chain (Fig. 3) relating the space groups of both the high- and the low-temperature structures

$$u_\alpha(l, \kappa) = \sum_Z \sum_i C^Z(i)\xi_\alpha^Z(\kappa, l|i),$$

where the first sum is over all possible space groups Z that appear in the group–subgroup chain (Fig. 3), such that $G > Z > H$, including the trivial case G and H. $u_\alpha(l, \kappa)$ is

Figure 7
Histograms showing the amplitudes of the displacements of the chain-adapted symmetry modes for atoms at Wyckoff positions 4(a) in the cubic ($P2_13$) phase.
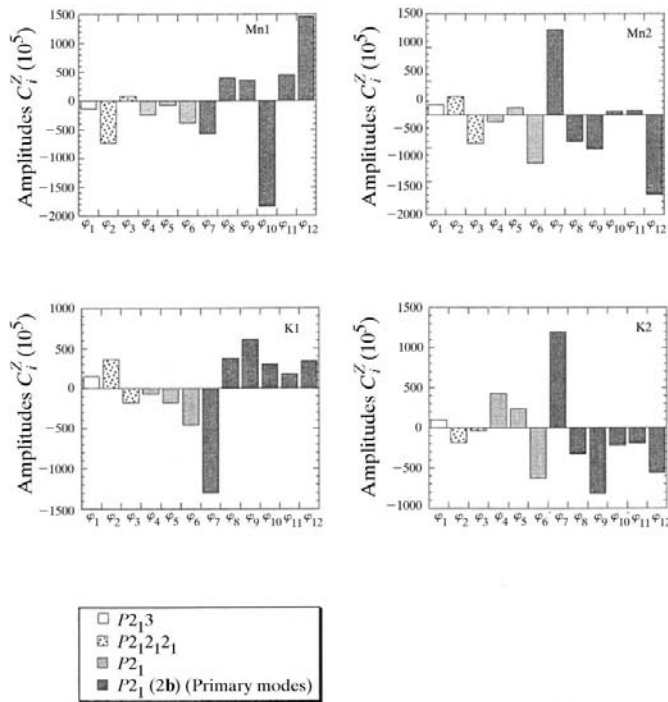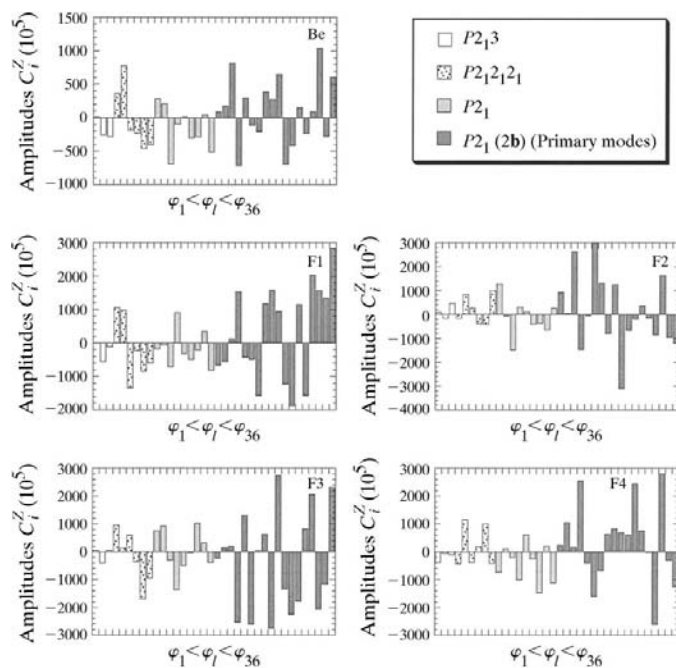

Figure 8
Histograms showing the amplitudes of the displacements of the chain-adapted symmetry modes for atoms at Wyckoff poistions 12(b) in the cubic ($P2_13$) phase.

Table 7
Chain-adapted symmetry modes compatible with the $P2_13$ ($b' = 2b$) symmetry for atoms in the $12(b)$ Wyckoff position of the $P2_1$ space group.

The first 12 atoms and the second 12 atoms are listed following the labelling scheme of the *International Tables for Crystallography* (1992, Vol. A). Each group of 12 atoms belong to a cubic unit cell. Atomic positions are given in full as footnotes.

Atomic positions	$P2_13$ modes			$P2_12_12_1$ modes						$P2_1$ modes								
	ϕ_1	ϕ_2	ϕ_3	ϕ_4	ϕ_5	ϕ_6	ϕ_7	ϕ_8	ϕ_9	ϕ_{10}	ϕ_{11}	ϕ_{12}	ϕ_{13}	ϕ_{14}	ϕ_{15}	ϕ_{16}	ϕ_{17}	ϕ_{18}
Zero cell																		
(1)	100	010	001	100	010	001	000	000	000	100	010	001	000	000	000	000	000	000
(2)	$\bar{1}$00	0$\bar{1}$0	001	$\bar{1}$00	0$\bar{1}$0	001	000	000	000	$\bar{1}$00	0$\bar{1}$0	001	000	000	000	000	000	000
(3)	$\bar{1}$00	010	00$\bar{1}$	$\bar{1}$00	010	00$\bar{1}$	000	000	000	100	0$\bar{1}$0	001	000	000	000	000	000	000
(4)	100	0$\bar{1}$0	00$\bar{1}$	100	0$\bar{1}$0	00$\bar{1}$	000	000	000	$\bar{1}$00	010	001	000	000	000	000	000	000
(5)	010	001	100	$0\tfrac12 0$	$00\tfrac12$	$\overline{\tfrac12}00$	010	001	100	000	000	000	100	010	001	000	000	000
(6)	0$\bar{1}$0	00$\bar{1}$	100	$0\overline{\tfrac12}0$	$00\tfrac12$	$\overline{\tfrac12}00$	0$\bar{1}$0	00$\bar{1}$	100	000	000	000	$\bar{1}$00	010	001	000	000	000
(7)	0$\bar{1}$0	001	$\bar{1}$00	$0\overline{\tfrac12}0$	$00\tfrac12$	$\tfrac12 00$	0$\bar{1}$0	001	$\bar{1}$00	000	000	000	$\bar{1}$00	0$\bar{1}$0	001	000	000	000
(8)	010	00$\bar{1}$	$\bar{1}$00	$0\tfrac12 0$	$00\tfrac12$	$\tfrac12 00$	010	00$\bar{1}$	$\bar{1}$00	000	000	000	100	0$\bar{1}$0	001	000	000	000
(9)	001	100	010	$00\tfrac12$	$\overline{\tfrac12}00$	$0\tfrac12 0$	00$\bar{1}$	$\bar{1}$00	0$\bar{1}$0	000	000	000	000	000	000	100	010	001
(10)	00$\bar{1}$	$\bar{1}$00	010	$00\tfrac12$	$\overline{\tfrac12}00$	$0\overline{\tfrac12}0$	001	100	0$\bar{1}$0	000	000	000	000	000	000	100	0$\bar{1}$0	001
(11)	00$\bar{1}$	100	0$\bar{1}$0	$00\overline{\tfrac12}$	$\tfrac12 00$	$0\tfrac12 0$	001	$\bar{1}$00	010	000	000	000	000	000	000	$\bar{1}$00	010	001
(12)	001	$\bar{1}$00	0$\bar{1}$0	$00\overline{\tfrac12}$	$\tfrac12 00$	$0\tfrac12 0$	00$\bar{1}$	100	010	000	000	000	000	000	000	$\bar{1}$00	0$\bar{1}$0	001
+t(0, 1, 0)																		
(13)	100	010	001	100	010	001	000	000	000	100	010	001	000	000	000	000	000	000
(14)	$\bar{1}$00	0$\bar{1}$0	001	$\bar{1}$00	0$\bar{1}$0	001	000	000	000	$\bar{1}$00	0$\bar{1}$0	001	000	000	000	000	000	000
(15)	$\bar{1}$00	010	00$\bar{1}$	$\bar{1}$00	010	00$\bar{1}$	000	000	000	100	0$\bar{1}$0	001	000	000	000	000	000	000
(16)	100	0$\bar{1}$0	00$\bar{1}$	100	0$\bar{1}$0	00$\bar{1}$	000	000	000	$\bar{1}$00	010	001	000	000	000	000	000	000
(17)	010	001	100	$0\overline{\tfrac12}0$	$00\overline{\tfrac12}$	$\tfrac12 00$	010	001	100	000	000	000	100	010	001	000	000	000
(18)	0$\bar{1}$0	00$\bar{1}$	100	$0\tfrac12 0$	$00\overline{\tfrac12}$	$\tfrac12 00$	0$\bar{1}$0	00$\bar{1}$	100	000	000	000	$\bar{1}$00	010	001	000	000	000
(19)	0$\bar{1}$0	001	$\bar{1}$00	$0\tfrac12 0$	$00\overline{\tfrac12}$	$\overline{\tfrac12}00$	0$\bar{1}$0	001	$\bar{1}$00	000	000	000	$\bar{1}$00	0$\bar{1}$0	001	000	000	000
(20)	010	00$\bar{1}$	$\bar{1}$00	$0\overline{\tfrac12}0$	$00\overline{\tfrac12}$	$\overline{\tfrac12}00$	010	00$\bar{1}$	$\bar{1}$00	000	000	000	100	0$\bar{1}$0	001	000	000	000
(21)	001	100	010	$00\overline{\tfrac12}$	$\tfrac12 00$	$0\overline{\tfrac12}0$	00$\bar{1}$	$\bar{1}$00	0$\bar{1}$0	000	000	000	000	000	000	100	010	001
(22)	00$\bar{1}$	$\bar{1}$00	010	$00\overline{\tfrac12}$	$\tfrac12 00$	$0\tfrac12 0$	001	100	0$\bar{1}$0	000	000	000	000	000	000	100	0$\bar{1}$0	001
(23)	00$\bar{1}$	100	0$\bar{1}$0	$00\tfrac12$	$\overline{\tfrac12}00$	$0\overline{\tfrac12}0$	001	$\bar{1}$00	010	000	000	000	000	000	000	$\bar{1}$00	010	001
(24)	001	$\bar{1}$00	0$\bar{1}$0	$00\tfrac12$	$\overline{\tfrac12}00$	$0\overline{\tfrac12}0$	00$\bar{1}$	100	010	000	000	000	000	000	000	$\bar{1}$00	0$\bar{1}$0	001
N	$(1/24)^{1/2}$	$(1/24)^{1/2}$	$(1/24)^{1/2}$	$(1/12)^{1/2}$	$(1/12)^{1/2}$	$(\bar{1}/12)^{1/2}$	$(1/16)^{1/2}$	$(1/16)^{1/2}$	$(1/16)^{1/2}$	$(1/8)^{1/2}$	$(1/8)^{1/2}$	$(1/8)^{1/2}$	$(1/8)^{1/2}$	$(1/8)^{1/2}$	$(1/8)^{1/2}$	$(1/8)^{1/2}$	$(1/8)^{1/2}$	$(1/8)^{1/2}$

Atomic positions	$P2_1(2b)$ modes																	
	ϕ_{19}	ϕ_{20}	ϕ_{21}	ϕ_{22}	ϕ_{23}	ϕ_{24}	ϕ_{25}	ϕ_{26}	ϕ_{27}	ϕ_{28}	ϕ_{29}	ϕ_{30}	ϕ_{31}	ϕ_{32}	ϕ_{33}	ϕ_{34}	ϕ_{35}	ϕ_{36}
Zero cell																		
(1)	100	010	001	000	000	000	000	000	000	000	000	000	000	000	000	000	000	000
(2)	$\bar{1}$00	0$\bar{1}$0	001	000	000	000	000	000	000	000	000	000	000	000	000	000	000	000
(3)	000	000	000	100	010	001	000	000	000	000	000	000	000	000	000	000	000	000
(4)	000	000	000	$\bar{1}$00	0$\bar{1}$0	001	000	000	000	000	000	000	000	000	000	000	000	000
(5)	000	000	000	000	000	000	100	010	001	000	000	000	000	000	000	000	000	000
(6)	000	000	000	000	000	000	000	000	000	100	010	001	000	000	000	000	000	000
(7)	000	000	000	000	000	000	$\bar{1}$00	0$\bar{1}$0	001	000	000	000	000	000	000	000	000	000
(8)	000	000	000	000	000	000	000	000	000	$\bar{1}$00	0$\bar{1}$0	001	000	000	000	000	000	000
(9)	000	000	000	000	000	000	000	000	000	000	000	000	100	010	001	000	000	000
(10)	000	000	000	000	000	000	000	000	000	000	000	000	000	000	000	100	010	001
(11)	000	000	000	000	000	000	000	000	000	000	000	000	000	000	000	$\bar{1}$00	0$\bar{1}$0	001
(12)	000	000	000	000	000	000	000	000	000	000	000	000	$\bar{1}$00	0$\bar{1}$0	001	000	000	000
+t(0, 1, 0)																		
(13)	$\bar{1}$00	0$\bar{1}$0	00$\bar{1}$	000	000	000	000	000	000	000	000	000	000	000	000	000	000	000
(14)	100	010	00$\bar{1}$	000	000	000	000	000	000	000	000	000	000	000	000	000	000	000
(15)	000	000	000	$\bar{1}$00	0$\bar{1}$0	00$\bar{1}$	000	000	000	000	000	000	000	000	000	000	000	000
(16)	000	000	000	100	010	00$\bar{1}$	000	000	000	000	000	000	000	000	000	000	000	000
(17)	000	000	000	000	000	000	$\bar{1}$00	0$\bar{1}$0	00$\bar{1}$	000	000	000	000	000	000	000	000	000
(18)	000	000	000	000	000	000	000	000	000	$\bar{1}$00	0$\bar{1}$0	00$\bar{1}$	000	000	000	000	000	000
(19)	000	000	000	000	000	000	100	010	00$\bar{1}$	000	000	000	000	000	000	000	000	000
(20)	000	000	000	000	000	000	000	000	000	100	010	00$\bar{1}$	000	000	000	000	000	000
(21)	000	000	000	000	000	000	000	000	000	000	000	000	$\bar{1}$00	0$\bar{1}$0	00$\bar{1}$	000	000	000
(22)	000	000	000	000	000	000	000	000	000	000	000	000	000	000	000	$\bar{1}$00	0$\bar{1}$0	00$\bar{1}$
(23)	000	000	000	000	000	000	000	000	000	000	000	000	000	000	000	100	010	00$\bar{1}$
(24)	000	000	000	000	000	000	000	000	000	000	000	000	100	010	00$\bar{1}$	000	000	000
N	$\tfrac12$	$\tfrac12$	$\tfrac12$	$\tfrac12$	$\tfrac12$	$\tfrac12$	$\tfrac12$	$\tfrac12$	$\tfrac12$	$\tfrac12$	$\tfrac12$	$\tfrac12$	$\tfrac12$	$\tfrac12$	$\tfrac12$	$\tfrac12$	$\tfrac12$	$\tfrac12$

(1) x, y, z; (2) $\tfrac12 - x, -y, \tfrac12 + z$; (3) $-x, \tfrac12 + y, \tfrac12 - z$; (4) $\tfrac12 + x, \tfrac12 - y, -z$; (5) z, x, y; (6) $\tfrac12 + z, \tfrac12 - x, -y$; (7) $\tfrac12 - z, -x, \tfrac12 + y$; (8) $-z, \tfrac12 + x, \tfrac12 - y$; (9) y, z, x; (10) $-y, \tfrac12 + z, \tfrac12 - x$; (11) $\tfrac12 + y, \tfrac12 - z, -x$; (12) $\tfrac12 - y, -z, \tfrac12 + x$; (13) $x, y + 1, z$; (14) $\tfrac12 - x, -y + 1, \tfrac12 + z$; (15) $-x, \tfrac12 + y + 1, \tfrac12 - z$; (16) $-x, \tfrac12 + y + 1, \tfrac12 - z$; (16) $\tfrac12 + x, \tfrac12 - y + 1, -z$; (17) $z, x + 1, y$; (18) $\tfrac12 + z, \tfrac12 - x + 1, -y$; (19) $\tfrac12 - z, -x + 1, \tfrac12 + y$; (20) $-z, \tfrac12 + x + 1, \tfrac12 - y$; (21) $y, z + 1, x$; (22) $-y, \tfrac12 + z + 1, \tfrac12 - x$; (23) $\tfrac12 + y, \tfrac12 - z + 1, -x$; (24) $\tfrac12 - y, -z + 1, \tfrac12 + x$.

the displacement of each atom (l,κ) in the low-symmetry structure, where l represents a unit cell of the high-symmetry structure, κ an atomic label within the corresponding unit cell and α represents the three independent components (x, y, z). ξ and C are the polarization vector and the amplitude of the symmetry mode. For each space group Z, several modes can exist in the decomposition and the index i runs over them.

The basic procedure of this method is explained in Aroyo & Pérez-Mato (1998). For the four atoms in special positions (K1, K2, Mn1 and Mn2) there are 12 chain-adapted symmetry modes: one $P2_13$ (φ_1), two $P2_12_12_1$ (φ_2, φ_3), three $P2_1$ (φ_4–φ_6) and six $P2_1(2\mathbf{b})$ (φ_7–φ_{12}). Their polarization vectors are listed in Table 6. For the remaining five atoms occupying general positions there are 36 symmetry modes: three $P2_13$ (ϕ_1–ϕ_3), six $P2_12_12_1$ (ϕ_4–ϕ_9), nine $P2_1$ (ϕ_{10}–ϕ_{18}) and 18 $P2_1(2\mathbf{b})$ (ϕ_{19}–ϕ_{36}). Their polarization vectors are given in Table 7. The weight of each of these modes in the total distortion can be calculated by Fourier analysis. To determine the displacement field the atomic coordinates of the monoclinic and cubic structures are compared. Owing to the doubling of the monoclinic unit cell, two consecutive cubic unit cells along the $\mathbf{b}$ direction must be considered.

Figs. 7 and 8 show the amplitudes of the symmetry-adapted modes for atoms in special and general positions, respectively. Note that in the monoclinic distortion, some of the amplitudes of the primary symmetry modes (φ_7–φ_{12} and ϕ_{18}–ϕ_{36}) have much higher values than those of the secondary ones (φ_1–φ_6 and ϕ_1–ϕ_{18}). Nevertheless, some secondary modes have a significant contribution to the global atomic displacement (see, for instance, Fig. 8 corresponding to atoms in general positions). In the case of atoms in special positions, the weight of the primary modes for some atoms is especially important.

4. Conclusions

This is the first work reporting a phase transition in tetra-fluoroberyllate langbeinites as well as a new type of low-temperature structure within the family of langbeinites. The phase transition in KMnB is accompanied by the doubling of the $\mathbf{b}$ axis. The space group of this low-temperature phase has been determined using X-ray diffraction and optical observation of the domain pattern. In spite of the complicated domain structure, the low-temperature monoclinic structure has been determined and analysed.

The resolution of the monoclinic structure of KMnB has revealed some factors which can be considered as responsible for the $P2_13 \leftrightarrow P2_1$ ($b' = 2b$) phase transition. On one hand, the rotations of the BeF_4 tetrahedra make the coordination of the monovalent K atoms different from that at room temperature and that observed in the orthorhombic phases of KMnS and KCdS (Abrahams *et al.*, 1978; Yamada, Maeda & Adachi, 1981). On the other hand, these rotations seem to provoke the unit-cell doubling along the $\mathbf{b}$ axis, since two tetrahedra occupying translationally equivalent positions in two consecutive cubic unit cells along $\mathbf{b}$ rotate in opposite

senses. The symmetry mode analysis shows that not only the primary modes are important, but the secondary modes also have significant contributions to the monoclinic distortions.

In the seventies it was established that the size of the monovalent cation is responsible for the different phase transition schemes (consider for instance the case of TCdS and KCdS) in langbeinites. Later, it was proved experimentally that a change in the divalent cation, leaving the monovalent cation intact, provokes a change in the phase transition sequence [cases of KCdS, KMnS and KCoS, KZnS (Abrahams & Bernstein, 1977; Hikita *et al.*, 1978; Yamada *et al.*, 1980; Hikita *et al.*, 1980; Yamada, Hikita & Yamada, 1981; Maeda & Ikeda, 1981)]. The present work has revealed that also the tetrahedral groups play a very important role in the phase transition sequence of some langbeinites.

References

Abrahams, S. C. & Bernstein, J. L. (1977). *J. Chem. Phys.* **67**, 2146–2150.

Abrahams, S. C., Lissalde, F. & Bernstein, J. L. (1978). *J. Chem. Phys.* **68**, 1926–1935.

Aleonard, S. & Le Fur, Y. (1967). *Bull. Soc. Fr. Minéral. Cristallogr.* **90**, 168–171.

Aroyo, M. I. & Pérez-Mato, J. M. (1998). *Acta Cryst.* A**54**, 19–30.

Brese, N. E. & O'Keeffe, M. (1991). *Acta Cryst.* B**47**, 192–197.

Brezina, B. & Glogarova, M. (1972). *Phys. Status Solidi A*, **11**, K39–K42.

Brown, I. D. & Altermatt, D. (1985). *Acta Cryst.* B**41**, 244–247.

Cord, P. P., Courtine, P. & Pannetier, G. (1971). *Bull. Soc. Chim. Fr.* **7**, 2461–2465.

Cosier, J. & Glazer, A. M. (1986). *J. Appl. Cryst.* **19**, 105–107.

Dvorák, D. (1974). *Phys. Status Solidi B*, **66**, K87–K89.

Enraf–Nonius. (1989). *CAD*4 Software, Version 5.0. Enraf–Nonius, Delft, The Netherlands.

Glogarova, M., Fousek, J. & Brezina, B. (1972). *J. Physique*, **33**, C2, 75–78.

Genty, M., Le Fur, Y. & Aleonard, S. (1968). *Bull. Soc. Fr. Mineral. Cristallogr.* **91**, 237–241.

Guelylah, A., Aroyo, M. I. & Pérez-Mato, J. M. (1996). *Phase Transit.* **59**, 155–179.

Guelylah, A., Breczewski, T. & Madariaga, G. (1996). *Acta Cryst.* C**52**, 2951–2954.

Guelylah, A., Madariaga, G., Morgenroth, W., Aroyo, M. I., Breczewski, T. & Bocanegra E. H. (2000). *Acta Cryst.* B**56**, 921–935.

Hikita, T., Chubachi, Y. & Ikeda, T. (1978). *J. Phys. Soc. Jpn*, **44**, 525–528.

Hikita, T., Kitabatake, M. & Ikeda, T. (1980). *J. Phys. Soc. Jpn*, **49**, 1421–1428.

Jona, F. & Pepinsky, R. (1956). *Phys. Rev.* **103**, 1126–1130.

Kohler, V. K. & Franke, W. (1964). *Acta Cryst.* **17**, 1088–1089.

Le Fur, Y. & Aléonard, S. (1969). *Mater. Res. Bull.* **4**, 601–616.

Leclaire, A., Benmoussa, A., Borel, M. M., Grandin, A. & Raveau, B. (1989). *J. Solid State Chem.* **78**, 227–231.

Lissalde, F., Abrahams, S. C., Bernstein, J. L. & Nassau, K. (1979). *J. Appl. Phys.* **50**, 845–851.

Maeda, M. (1979). *J. Phys. Soc. Jpn*, **47**, 1581–1587.

Maeda, M. & Ikeda, T. (1981). *J. Phys. Soc. Jpn*, **50**, 1815–1816.

Petricek, V. & Dusek, M. (1998). *JANA*98. Institute of Physics. Academy of Sciences of the Czech Republic, Praha, Czech Republic.

research papers

Rae, D., Thompson, J. G., Withers, R. L. & Willis, A. (1990). *Acta Cryst.* B**46**, 447–487.

Rodriguez-Carvajal, J. (1990). *Fullprof*, Version 3.1c-jan96. Laboratoire Léon Brillouin (CEA-CNRS), Saclay, France.

Sapriel, J. (1975). *Phys. Rev. B*, **12**, 5128–5140.

Speer, D. & Salje, E. (1986). *Phys. Chem. Miner.* **13**, 17–24.

Yamada, N., Hikita, T., Maeda, M. & Ikeda. T. (1980). *J. Phys. Soc. Jpn*, **49** (Suppl. B), 102–106.

Yamada, N., Hikita, T. & Yamada, T. (1981). *Ferroelectrics*, **33**, 59–61.

Yamada, N., Maeda, M. & Adachi, H. (1981). *J. Phys. Soc. Jpn*, **50**, 907–913.